J Math Chem (2009) 45:188–222
DOI 10.1007/s10910-008-9376-5

ORIGINAL PAPER

Kinetics of phase transitions in two dimensional Ising models studied with the string method

Maddalena Venturoli · Eric Vanden-Eijnden · Giovanni Ciccotti

Received: 4 November 2007 / Accepted: 21 November 2007 / Published online: 17 May 2008

Abstract The kinetics of phase transitions in the two dimensional Ising model under different conditions is studied using the string method. The key idea is to work in collective variables, consisting of block of spins, which allow for a continuous approximation of the collective variable state-space. The string method computes the minimum free energy path (MFEP) in this collective variable space, which is shown to explain the mechanism of the phase transformation (in particular, an approximation of its committor function, its free energy and its transition state). In this paper the theoretical background of the technique as well as its computational aspects are discussed in details. The string method is then used to analyze phase transition in the Ising model with imposed boundary conditions and in a periodic system under an external field of increasing magnitude. In each case, the mechanism of the phase transformation is elucidated.

Keywords Minimum free energy path · String method · Sampling · Phase transition · Ising model

M. Venturoli (✉) · E. Vanden-Eijnden
Courant Institute of Mathematical Sciences, New York University, New York, NY 10012, USA
e-mail: mventuro@cims.nyu.edu

E. Vanden-Eijnden
e-mail: eve2@cims.nyu.edu

G. Ciccotti
Dipartimento di Fisica and CNISM, Unità di Roma 1, Università di Roma La Sapienza,
Piazzale Aldo Moro, 2, 00185 Roma, Italy
e-mail: giovanni.ciccotti@roma1.infn.it

1 Introduction

Nucleation events are ubiquitous in the kinetics of phase transitions and they are typically difficult to observe in computations. The reason is that these nucleation events are rare reactive events during which the system must find its way out of the metastable phase it is currently in, and towards the new more stable phase it reaches after transition. This involves going trough a dynamical bottleneck of energetic or entropic origin and, as a result, rare events are usually beyond reach of standard numerical simulations using molecular dynamics or even Monte Carlo methods. In addition, the mechanism of these rare events can be quite complicated, so much so that it would be difficult to analyze from actual reactive trajectories by which the event occurs even if these trajectories were available (typically, they are not).

A typical example of nucleation event during phase transition is the creation of a nucleus of critical size out of which the crystal phase can grow during a liquid-to-solid phase transition [1,2]. The size and shape of this nucleus are typically hard to describe because the critical nucleus may be much bigger than the individual molecules in the system and its properties depend only very indirectly on the potential energy between the molecules (i.e. they involve collective effects in which entropy may matter a lot). Similar difficulties arise in the Ising model in two-dimension which will be the focus of the present study. While this system is clearly a much idealized cartoon of an actual molecular system, it too exhibits the kinetics of a phase transition involving the creation of a nucleus which is much bigger in size than the lattice size of the system and whose shape involves a nontrivial interplay between entropic and energetic effects.

When attempting to describe the kinetics of a phase transition either in the Ising model or in more realistic systems, one typically faces a dilemma. On the one hand, one would like to introduce a suitable coarsened description of the system which would remove the irrelevant small-scales details of the transition and focus on its more robust large-scale characteristics. On the other hand if one coarsens the system too much, one typically oversimplifies things so much that the answer becomes unreliable. For instance, methods based on analyzing the free energy landscape in a very few collective variables to describe the nucleation events, like e.g. the radial size of the nucleus or its volume, typically fail at giving an accurate description of the way this nucleus forms in the system [3].

In this work, we propose a way to get around these difficulties using the string method in collective variables [4]. Unlike standard free energy based methods, the string method allows to use simultaneously a very large number of collective variables [5], thereby reducing (though not eliminating) the bias introduced by these variables (more on this below). The string method is a tool to compute the minimum free energy path (MFEP) in the collective variables which, if these variables are sufficient to describe the reaction, is also the path of maximum likelihood by which the transition occurs when observed in the collective variables. Along the MFEP, the state with maximum free energy is the transition state, i.e. the critical nucleus (or, more precisely, the ensemble of critical nuclei) from which the system has half-half probability to either fall back in the metastable phase or proceed towards the more stable phase and achieve the transition.

As mentioned above, the string method in collective variables still requires to choose these variables a priori. In the context of the Ising model, a rather natural choice is to use the average magnetization in blocks of spins as collective variables. When the system is big enough, these blocks can be taken quite large and still be numerous in the system, thereby allowing for a rather local description of the magnetization in the system which one expects has chances to be accurate enough (this, however, must be verified a posteriori by checking that the state of maximum free energy along the MFEP corresponds indeed to the critical nuclei). Using average magnetization in blocks of spins as collective variables has also another advantage, namely that these variables permit to approximate the state of the system by a continuous variable in $\mathbb{R}^{M_B}$ if M_B is the number of blocks. In contrast, the state-space of the original Ising model is discrete, and we will see that the discrete-to-continuous approximation results in an enormous simplification in computational complexity while accurately predicting the mechanism of the transition.

The remainder of this paper is organized as follows. In Sect. 2 we recall the main features of the Ising model. We also specify the dynamics of this system, which is important since, unlike the thermodynamic properties of the system (e.g. the average magnetization per spin), the mechanism and timing of the phase transition in the Ising model do depend on the specific dynamics that we use. Section 3 contains the theory behind our approach, and it is divided in several subsections. First, in Sect. 3.1 we recall the main results of transition path theory (TPT) [6,7] which gives exact explicit expressions for various quantities characterizing the statistical properties of the reactive trajectories (i.e. the trajectories by which the transition occurs) in terms of the equilibrium probability distribution of the system (which is known) and the so-called committor function (which is unknown but solves a variational problem). In Sect. 3.2 we introduce the collective variables as a way to simplify this variational problem. We also show that the discrete-to-continuum approximation offers a connection with the results of Ref. [4]; in particular, it indicates how to define the MFEP in the Ising model and why this MFEP is relevant, two topics which are discussed in Sect. 3.3. Finally in Sect. 3.4 we recall how the string method can be used to calculate the MFEP. We then proceed to apply these results to the Ising model in Sect. 4. There we first validate numerically the discrete-to-continuum approximation (Sect. 4.1); then we consider a situation with no applied field in which the mechanism of transition is dictated by the boundary conditions imposed on the system (Sect. 4.2); and finally we consider situations with periodic boundary conditions with an applied field of increasing magnitude (Sect. 4.3) and study the way the mechanism of the transition depends on the field (as we will see this mechanism also depends on the size of the system, and we study the nontrivial interplay between finite size effects and applied field). This last example brings out several interesting features of our approach which are discussed in the concluding Sect. 5. This section also contains several speculations as well as suggestions for future work, consistent with the present paper being very much in the spirit of an exploratory paper in which our answers to the original questions open many new ones.

2 Model

In this section, we recall the main ingredients of the two-dimensional Ising model with nearest neighbor interactions. The system consists of N_s spins which can each take values ± 1 and are located at the vertices of a regular square lattice. Thus, the state-space of the system is $S = \{-1, 1\}^{N_s}$, and elements in this space will be denoted by $\sigma = (\sigma_1, \sigma_2, \ldots, \sigma_{N_s}) \in S$, where $\sigma_j = \pm 1$ is the value of the spin at site j. The Hamiltonian of the system is

$$H(\sigma) = -J \sum_{\langle i,j \rangle} \sigma_i \sigma_j - h \sum_{i=1}^{N_s} \sigma_i \tag{1}$$

where $J > 0$ is the coupling constant between the spins, h is a uniform external magnetic field, and $\langle i, j \rangle$ indicates that the sum runs only over spin pairs which are nearest neighbors.

2.1 Equilibrium properties

The equilibrium probability distribution of the system is

$$\mu(\sigma) = Z^{-1} e^{-\beta H(\sigma)}, \qquad Z = \sum_{\sigma \in S} e^{-\beta H(\sigma)} \tag{2}$$

where $1/\beta$ is the temperature. It is known that, in dimension two and higher, the Ising model undergoes a phase transition between a disordered and an ordered phase (see e.g. [8,9]). When the temperature $1/\beta$ is below a critical temperature $1/\beta_c$, the distribution (2) is bimodal and sharply peaked around two metastable states with spontaneous magnetization per spin $\mathrm{m} = N_s^{-1} \sum_{i=1}^{N_s} \sigma_i \to \pm 1$ as $1/\beta \to 0$. In contrast, when $1/\beta > 1/\beta_c$ the distribution is mono-modal and broader, and $\mathrm{m} \approx 0$. For the two-dimensional Ising model in the absence of a magnetic field ($h = 0$), $1/\beta_c \approx 2.269 J$ and the spontaneous magnetization per spin at $1/\beta < 1/\beta_c$ is given by Onsager–Yang expression [10,11]

$$\mathrm{m} = \left(1 - (\sinh(2\beta J))^{-4}\right)^{1/8}. \tag{3}$$

This expression is plotted in Fig. 1 and compared with the results of a Monte Carlo simulation of a system of $N_s = 100^2$ spins with periodic boundary conditions and $h = 0$. How this Monte Carlo simulation was performed is described next.

2.2 Dynamics

Since we are interested in the kinetics of the phase transition in the Ising model, we need to specify a dynamics. Indeed, while many such dynamics exist which are

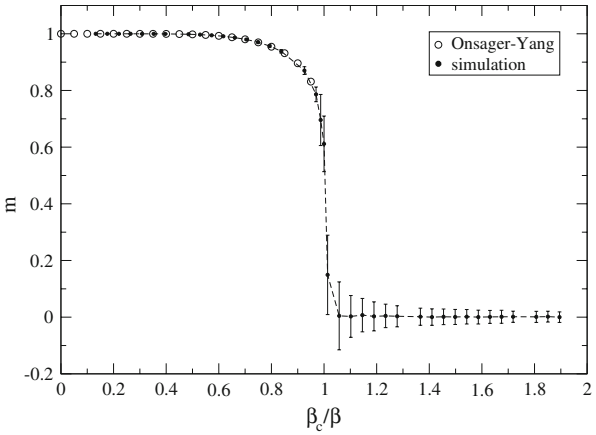

Fig. 1 Spontaneous magnetization per spin as a function of temperature in the two-dimensional Ising model with nearest neighbor interactions at zero external field. The open circles (only for $1/\beta < 1/\beta_c$) are calculated using the Onsager–Yang analytical expression in (3) while the full circles are the simulation results. Note the larger error bars as $1/\beta \to 1/\beta_c$, which reflect the fact that the fluctuations in the system grow as the temperature approaches the critical temperature $1/\beta_c$

consistent with the equilibrium distribution (2), the mechanism and timing of the transition between the metastable states when $1/\beta < 1/\beta_c$ depends on the specific dynamics that we choose. Here we will assume that in any time interval $[t, t + dt]$, every spin σ_j in the system independently attempts to flip with probability $dt + o(dt)$, and the probability of success of this attempt is given by

$$c(\sigma, \sigma^j) = \min\left\{e^{-\beta(H(\sigma^j)-H(\sigma))}, 1\right\} \tag{4}$$

where $H(\sigma)$ is the Hamiltonian defined in (1) and σ^j is the state of the system obtained from σ by flipping spin σ_j, i.e.

$$\sigma_i^j = \begin{cases} \sigma_i & \text{if} \quad i \neq j \\ -\sigma_i & \text{if} \quad i = j \end{cases} \tag{5}$$

The factor (4) is the standard Metropolis acceptance/rejection factor and it leads to a dynamics which can be easily simulated by Monte Carlo. Given that a spin has attempted (successfully or not) to flip at time t_n, the next flipping attempt occurs at time $t_n + \tau$ where τ is a random variable distributed exponentially according to

$$\text{prob}(\tau \leq t) = 1 - \exp(-N_s t). \tag{6}$$

This attempt involves a spin σ_j chosen at random in the system and succeeds with probability (4). The cycle then repeats itself.

The dynamics specified above is that of a continuous-time Markov chain with (2) as unique equilibrium distribution and which satisfies detailed balance

$$\mu(\sigma)c(\sigma,\sigma^j)=\mu(\sigma^j)c(\sigma^j,\sigma). \tag{7}$$

This condition is equivalent to the time-reversibility of the Markov chain.

3 Theoretical and computational aspects

In this section, we collect all the theoretical and computational results that we will then use in Sect. 4 to study specific examples of phase transformations in the Ising model. Since this section is quite long and rather technical, it is useful to give the main upshots upfront. In essence, we show how to define the MFEP in the context of the Ising model, that is, a continuous curve in the space of some appropriate collective variables which allows to understand the mechanism of the phase transformation (specifically: to determine the committor function for this transformation as well as its free energy and its rate). We also show how to identify the MFEP in practice using the string method.

3.1 Transition path theory for Markov jump processes

We are primarily interested in understanding the mechanism of the transitions which occur when $1/\beta < 1/\beta_c$ between the metastable states with magnetization $\pm$m. One way to formalize this question is via transition path theory (TPT) developed in [12] (see also [6,7]) for stochastic differential equations, and generalized in [13] to the case of continuous-time Markov processes on a discrete state-space. The main results of TPT in the context of the Ising model are summarized next.

The metastable sets which exist when $1/\beta < 1/\beta_c$, can be characterized e.g. as the two sets $A \subset S$ and $B \subset S$ such that

$$A=\left\{\sigma : \frac{1}{N_s}\sum_{j=1}^{N_s}\sigma_j < -\mathrm{m}+\delta\right\} \qquad B=\left\{\sigma : \frac{1}{N_s}\sum_{j=1}^{N_s}\sigma_j > \mathrm{m}-\delta\right\} \tag{8}$$

where $\delta > 0$ is a small parameter. Thus A and B are two sets containing spin configurations close to the one where the spontaneous magnetization is $-$m or m respectively. When $1/\beta < 1/\beta_c$ and N_s is large, one expects that the system will revisit many times either A or B before making a transition between A and B. Eventually, however, such a transition will occur and one is interested in characterizing how and when. More precisely, given an infinitely long dynamical trajectory of the system, we can prune out of this trajectory all the pieces during which a transition does occur, i.e. all the pieces during which the system is out of A and B and is such that it came from A last and will go to B next (or came from B last and will go to A next: the dynamics being time reversible because of (7), either pieces of the trajectory are statistically equivalent after time reversal). We call these pieces "reactive trajectories," and we are interested in understanding their statistical properties. The key result of TPT is that these statistical properties can all be expressed in terms of the equilibrium probability distribution (2) and the so-called committor function $q(\sigma)$ defined such that

$$q(\sigma) = \begin{pmatrix} \text{probability that the system initiated in state } \sigma \\ \text{will reach } B \text{ rather than } A \text{ next} \end{pmatrix}. \tag{9}$$

In particular, the probability $\mu_R(\sigma)$ to observe a reactive trajectory at state σ is simply

$$\mu_R(\sigma) = \mu(\sigma)q(\sigma)(1 - q(\sigma)) \tag{10}$$

expressing the fact that, using the Markov property, $\mu_R(\sigma)$ is the probability to observe any trajectory (reactive or not) at state σ (which is $\mu(\sigma)$) times the probability that it is reactive (i.e that it will go to B next and came from A last which, by time reversibility, is $q(\sigma)(1 - q(\sigma))$). Thus, the probability to observe a reactive trajectory is

$$Z_R = \sum_{\sigma \in S} \mu_R(\sigma) < 1; \tag{11}$$

TPT also gives the following expressions for the probability current of reactive trajectories flowing from state σ to state σ^j [13]

$$f(\sigma, \sigma^j) = \begin{cases} \mu(\sigma)c(\sigma, \sigma^j)\left(q(\sigma^j) - q(\sigma)\right) & \text{if } q(\sigma^j) > q(\sigma) \\ 0 & \text{otherwise} \end{cases} \tag{12}$$

and for the mean frequency of appearance of reactive trajectories (i.e. the rate of the transition)

$$k_R = \frac{1}{2} \sum_{j=1}^{N_s} \sum_{\sigma \in S} \mu(\sigma)c(\sigma, \sigma^j)\left(q(\sigma^j) - q(\sigma)\right)^2 \tag{13}$$

where $c(\sigma, \sigma^j)$ is the transition matrix defined in (4). For the derivation of (12) and (13), we refer the reader to [13].

To make these results complete, it remains to specify an equation for the committor function $q(\sigma)$. This equation is [13]

$$\begin{cases} (Lq)(\sigma) = 0 & \text{if } \sigma \notin A \cup B \\ q(\sigma) = 0 & \text{if } \sigma \in A \\ q(\sigma) = 1 & \text{if } \sigma \in B, \end{cases} \tag{14}$$

where L is the so-called infinitesimal generator of the Markov chain (also known as the transition rate matrix), here given by

$$(Lq)(\sigma) = \sum_{j=1}^{N_s} c(\sigma, \sigma^j)(q(\sigma^j) - q(\sigma)). \tag{15}$$

For future use, note that (14) admits a variational formulation. Indeed, it can be checked by a direct calculation using the detailed balance condition (7) (see the end of this section) that (14) is the Euler Lagrange equation satisfied by the minimizer of

$$I(q) = \frac{1}{2} \sum_{j=1}^{N_s} \sum_{\sigma \in S} \mu(\sigma) c(\sigma, \sigma^j) \left(q(\sigma^j) - q(\sigma) \right)^2 \tag{16}$$

where the minimization is sought over all $q(\sigma)$ which are 0 if $\sigma \in A$ and 1 if $\sigma \in B$.

Summarizing, the mechanism and the rate of the dynamical transition in the Ising model can be quantified by (10), (11), (12) and (13). These expressions, however, require one to calculate the committor function $q(\sigma)$ via solution of (15) which, when N_s is large, is very challenging because of the enormous size of the state space $S = \{-1, 1\}^{N_s}$. The main objective of this paper is to design an approximate way to solve (14) and obtain an estimate for $q(\sigma)$ which can then be used in (10), (11), (12) and (13).

Derivation of (15). (16) can be written as

$$I(q) = \frac{1}{2} \sum_{\substack{\sigma', \sigma'' \in S \\ |\sigma' - \sigma''| = 2}} \mu(\sigma') c(\sigma', \sigma'') \left(q(\sigma'') - q(\sigma') \right)^2 . \tag{17}$$

Taking the derivative of (17) with respect to $q(\sigma)$ we obtain:

$$\begin{aligned} \frac{\delta I(q)}{\delta q(\sigma)} &= \sum_{\substack{\sigma', \sigma'' \in S \\ |\sigma' - \sigma''| = 2}} \mu(\sigma') c(\sigma', \sigma'') (q(\sigma'') - q(\sigma')) (\delta_{\sigma''=\sigma} - \delta_{\sigma'=\sigma}) \\ &= \sum_{\substack{\sigma' \in S \\ |\sigma' - \sigma| = 2}} \mu(\sigma') c(\sigma', \sigma) (q(\sigma) - q(\sigma')) \\ &\quad - \sum_{\substack{\sigma'' \in S \\ |\sigma - \sigma''| = 2}} \mu(\sigma) c(\sigma, \sigma'') (q(\sigma'') - q(\sigma)). \end{aligned} \tag{18}$$

In the first term we can use detailed balance to replace $\mu(\sigma')c(\sigma', \sigma)$ by $\mu(\sigma)c(\sigma, \sigma')$ and in the second term we can relabel σ'' into σ' to arrive at

$$\begin{aligned} \frac{\delta I(q)}{\delta q(\sigma)} &= -2\mu(\sigma) \sum_{\substack{\sigma' \in S \\ |\sigma - \sigma'| = 2}} c(\sigma, \sigma') (q(\sigma') - q(\sigma)) \\ &= -2\mu(\sigma) \sum_{j=1}^{N_s} c(\sigma, \sigma^j) (q(\sigma^j) - q(\sigma)). \end{aligned} \tag{19}$$

Equating to 0 the right hand side of this equation and dividing by $-2\mu(\sigma)$ gives (14).

3.2 Collective variables and continuous approximation of the committor function

To simplify the problem, we shall suppose that we can introduce a set of collective variables, defined on S, which are appropriate to describe the mechanism of the reaction in that they are sufficient to parametrize $q(\sigma)$. This assumption will be verified a posteriori.

These collective variables are constructed in the following manner (see Fig. 2). The system is divided into M_B non-overlapping blocks $B_1, \ldots, B_{M_B}$, of equal size, and containing each N_s^B spins such that $M_B = N_s/N_s^B$. The collective variables are then defined as the local magnetization in each block, i.e.

$$\theta_\alpha(\sigma) = \frac{1}{N_s^B} \sum_{j \in J_\alpha} \sigma_j \tag{20}$$

where J_α denotes the set of indexes j such that $\sigma_j \in B_\alpha$ if $j \in J_\alpha$. One key approximation that we shall make is that the committor function $q(\sigma)$ can be parametrized approximately by the collective variables $\theta(\sigma) = (\theta_1(\sigma), \ldots, \theta_{M_B}(\sigma))$, i.e. there exists a function $Q(z)$ of $z = (z_1, \ldots, z_{M_B})$ such that

$$q(\sigma) \approx Q(\theta(\sigma)). \tag{21}$$

Inserting this ansatz in (16) leads to a new variational problem in which the following objective function must be minimized:

$$\hat{I}(Q) = \frac{1}{2} \sum_{\alpha=1}^{M_B} \sum_{j \in J_\alpha} \sum_{\sigma \in S} \mu(\sigma) c(\sigma, \sigma^j)(Q(\theta(\sigma^j)) - Q(\theta(\sigma))^2 \tag{22}$$

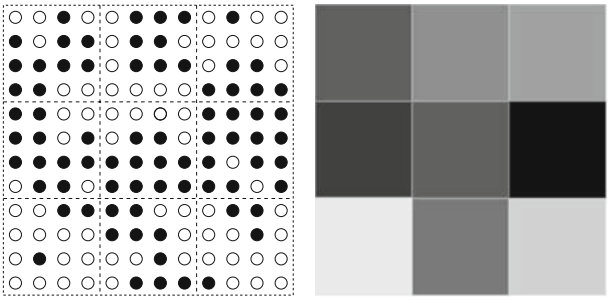

Fig. 2 Schematic representation of how the collective variables are constructed. A system of $N_s = 12 \times 12$ spins (left figure), represented by white (σ=1) and black (σ=−1) circles, is divided into $M_B = 9$ non-overlapping blocks, each containing $N_s^B = 16$ spins, and whose boundaries are shown by the dashed lines. The collective variables $\theta_\alpha(\sigma)$ are defined via (20) as the average value of the spins (i.e. the local magnetization) in each block B_α ($\alpha = 1, \ldots, M_B$). The figure on the right gives a pictorial representation of the values of collective variables for the spin configuration of the left figure. These values are represented using a grey-scale color coding (white=+1, black=−1)

where, for future use, we have split the sum over all the spins indexes j into a double sum over the blocks and over the spins in each block. Equation (22) must be minimized over all $Q(z)$ subject to $Q(z) = 0$ if $z \in a$ and $Q(z) = 1$ if $z \in b$, where a and b are the projections of the sets A and B in the space of the collective variables. The new variational problem is simpler than the original one, but still too complicated to be tackled directly.

To proceed further, we shall make another key approximation, namely that $Q(z)$ can be approximated by a function defined on a continuous state-space. The original $Q(z)$, of course, is defined on a discrete state-space since the collective variables $\theta_\alpha(\sigma)$ in (20) can only assume values which are integer multiples of $2/N_s^B$ between -1 and $+1$. However, when N_s^B is large, these variables represent a fine partition of the interval $[-1, 1]$, a property that we shall use next.

First let us rewrite (22) as

$$\hat{I}(Q) = \frac{1}{2} C^{-1} \int_{\mathbb{R}^{M_B}} \left(\sum_{\alpha=1}^{M_B} \sum_{j \in J_\alpha} \sum_{\sigma \in S} \mu(\sigma) c(\sigma, \sigma^j) e^{-\beta \frac{\lambda}{2} |\theta(\sigma) - z|^2} (Q(\theta(\sigma^j)) - Q(\theta(\sigma))^2 \right) dz \tag{23}$$

where $|\theta(\sigma) - z|^2 = \sum_{\alpha=1}^{M_B} (\theta_\alpha(\sigma) - z_\alpha)^2$, $\lambda > 0$ is a parameter whose role is explained below, and

$$C = \int_{\mathbb{R}^{M_B}} e^{-\beta \frac{\lambda}{2} |\theta(\sigma) - z|^2} dz = \left(\frac{2\pi}{\beta \lambda} \right)^{M_B/2}. \tag{24}$$

(23) is still strictly equivalent to (22), but we now make two approximations. To introduce the first, note that the summation in (23) only involves configurations which differ by only one spin. This implies that $\theta_\alpha(\sigma^j)$ and $\theta_\alpha(\sigma)$ differs by at most $2/N_s^B$ since $\theta_\alpha(\sigma^j) = \theta_\alpha(\sigma) \pm 2/N_s^B$ and $\theta_\beta(\sigma^j) = \theta_\beta(\sigma)$ for all $\beta \neq \alpha$ when spin σ_j by which σ^j and σ differ belongs to block B_α. Assuming that $Q(z)$ is relatively smooth on the scale $\Delta z_\alpha = 2/N_s^B$, we will approximate the finite difference $Q(\theta(\sigma^j)) - Q(\theta(\sigma))$ by a derivative, i.e.

$$Q(\theta(\sigma^j)) - Q(\theta(\sigma)) \approx \pm \frac{2}{N_s^B} \frac{\partial \bar{Q}(\theta(\sigma))}{\partial z_\alpha}. \tag{25}$$

where $\bar{Q}(z)$ is understood as the smooth interpolation on $z \in \mathbb{R}^{M_B}$ of the discrete $Q(\theta(\sigma))$ (i.e. $\bar{Q} : \mathbb{R}^{M_B} \to [0, 1]$ is smooth and such that $\bar{Q}(\theta(\sigma)) = Q(\theta(\sigma))$ for all possible values of $\theta(\sigma)$: see Fig. 3 for a schematic illustration).

In (25), $\partial \bar{Q}/\partial z_\alpha$ is still evaluated at $\theta(\sigma)$. The second approximation is to assume that $\partial \bar{Q}/\partial z_\alpha$ is approximately constant in the ball of radius $(\lambda\beta)^{-1/2}$ around $\theta(\sigma)$ on

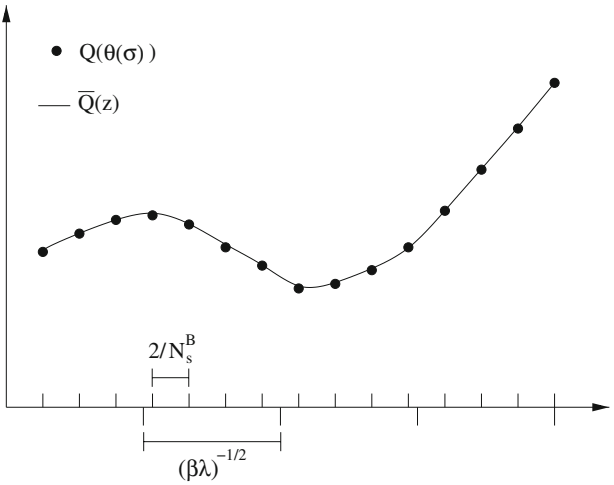

Fig. 3 $\bar{Q}(z)$ is the continuous interpolation of the committor, $Q(\theta(\sigma))$, defined on the discrete space of the collective variables

which the function $e^{-\beta\frac{\lambda}{2}|\theta(\sigma)-z|^2}$ is peaked, i.e.

$$\frac{\partial\,\bar{Q}(\theta(\sigma))}{\partial z_\alpha} \approx \frac{\partial\,\bar{Q}(z)}{\partial z_\alpha} \quad \text{for} \quad |z-\theta(\sigma)| \lesssim (\lambda\beta)^{-1/2}. \tag{26}$$

If this holds we can approximate $\bar{Q}(\theta(\sigma))$ by $\bar{Q}(z)$ under the integral in (23) and, after a little algebra, we are left with the following approximation of $\hat{I}(Q)$:

$$\hat{I}(Q) \approx \bar{I}(\bar{Q}) \equiv \frac{2}{(N_s^B)^2}\int_{\mathbb{R}^{M_B}} e^{-\beta F_\lambda(z)} \sum_{\alpha=1}^{M_B} m_\alpha^\lambda(z)\left(\frac{\partial\,\bar{Q}(z)}{\partial z_\alpha}\right)^2 dz. \tag{27}$$

Here we have introduced the "free energy" $F_\lambda(z)$ defined as

$$e^{-\beta F_\lambda(z)} = C^{-1}\sum_{\sigma\in S}\mu(\sigma)e^{-\beta\frac{\lambda}{2}|\theta(\sigma)-z|^2} \tag{28}$$

and the factor $m_\alpha^\lambda(z)$ defined as

$$m_\alpha^\lambda(z) \equiv \left\langle \sum_{j\in J_\alpha} c(\sigma,\sigma^j)\right\rangle_{\rho_{\lambda,z}} \tag{29}$$

where $\langle\cdot\rangle_{\rho_{\lambda,z}}$ denotes the average with respect to the distribution

$$\rho_{\lambda,z}(\sigma) = \frac{e^{-\beta\left(H(\sigma)+\frac{\lambda}{2}|\theta(\sigma)-z|^2\right)}}{\sum_{\sigma\in S} e^{-\beta\left(H(\sigma)+\frac{\lambda}{2}|\theta(\sigma)-z|^2\right)}}. \tag{30}$$

This is the equilibrium distribution function for the spin system in the extended Hamiltonian

$$H_{\lambda,z}(\sigma) = H(\sigma) + \frac{\lambda}{2}\sum_{\alpha=1}^{M_B}(\theta_\alpha(\sigma) - z_\alpha)^2 \tag{31}$$

and, for large λ, $\langle\cdot\rangle_{\rho_{\lambda,z}}$ approximates the equilibrium expectation conditional at $\theta(\sigma)=z$. Note also that the free energy $F_\lambda(z)$ is normalized in the sense that

$$\int_{\mathbb{R}^{M_B}} e^{-\beta F_\lambda(z)} = 1. \tag{32}$$

The objective function $\bar{I}(\bar{Q})$ in (27) is one of our main results since the analysis of the variational problem associated with this function will turn out to be much simpler than that of the original (16) or the reduced (22). Before explaining why this is the case, however, it is worth discussing in more details the validity of the approximations that led us to (27). As explained before, the ultimate check will consist in verifying that the minimizer of (27) is indeed a good approximation of the original committor function in the sense that (21) holds. But we can already state two necessary conditions for this to be the case. The first is that the resulting $\bar{Q}(z)$ should be mostly independent of the artificial parameter λ introduced in (23), at least in a certain range of values for λ. This, in turn, will require that the free energy $F_\lambda(z)$ and the factor $m_\alpha^\lambda(z)$ in (27) be also mostly independent of λ at least in some band of values of λ. This assumption will be verified later in Sect. 4.1. Here we simply note that this assumption is not unreasonable when N_s^B is large because in this case it is possible to satisfy

$$2/N_s^B < (\beta\lambda)^{-1/2}. \tag{33}$$

This inequality guarantees that $F_\lambda(z)$ and $m_\alpha^\lambda(z)$ are smooth functions of z because the factor $e^{-\beta\frac{\lambda}{2}|\theta(\sigma)-z|^2}$ in (28) and (29) smears out the features related to the discreteness of the collective variables (in contrast, as $\lambda\to\infty$, $F_\lambda(z)$ and $m_\alpha^\lambda(z)$ become zero except on the points in $[-1, 1]$ where z_α is a multiple of $2/N_s^B$ since these are the only admissible values for $\theta_\alpha(\sigma)$).

The second necessary condition is that the function $\bar{Q}(z)$ minimizing (27) should be smooth enough in order that (25) and (26) be valid. This requires that the next order terms in the expansion that led to (25) and (26) be negligible which, accounting for the inequality (33), reduces to the requirement that (see Fig. 3)

$$\frac{\sup_{z\in\mathbb{R}^{M_B}} ||\nabla_z\nabla_z \bar{Q}||}{\sup_{z\in\mathbb{R}^{M_B}} |\nabla_z \bar{Q}|} \ll (\beta\lambda)^{-1/2} \tag{34}$$

where $||\nabla_z\nabla_z \bar{Q}||$ denotes the norm of the Hessian tensor obtained by taking second derivatives of $\bar{Q}$ with respect to z, and $|\nabla_z \bar{Q}|$ is the norm of the gradient of $\bar{Q}$ with respect to z. This condition can be checked a posteriori.

Finally, we note that the continuous approximation above is consistent with attempts to approximate the dynamics of the Ising model by a partial differential equation in the limit when $N_s \to \infty$ and $N_s^B \to \infty$ with $N_s^B/N_s \to 0$. The existence of such limit can be rigorously proven in an Ising model with long range interaction, but it is left open for nearest neighbor interactions (see e.g. [14] and references therein).

3.3 Transition path of maximum likelihood

Let us now explain why the minimization of $\bar{I}(\bar{Q})$ in (27) is simpler than that of (22). In essence, this is because we can bypass this minimization altogether by observing the following. The Euler–Lagrange equation associated with the minimization of (27) is

$$\begin{cases} 0 = \displaystyle\sum_{\alpha=1}^{M_B} \frac{\partial}{\partial z_\alpha}\left(e^{-\beta F_\lambda(z)} m_\alpha^\lambda(z) \frac{\partial \bar{Q}}{\partial z_\alpha}\right), \\ \bar{Q}|_{z\in a} = 0, \quad \bar{Q}|_{z\in b} = 1. \end{cases} \tag{35}$$

This equation is the backward Kolmogorov equation for the committor function associated with the stochastic differential equation (e.g. [4])

$$\dot{z}_\alpha(\tau) = -m_\alpha^\lambda(z(\tau)) \frac{\partial F_\lambda(z(\tau))}{\partial z_\alpha} + \beta^{-1} \frac{\partial m_\alpha^\lambda(z(\tau))}{\partial z_\alpha} + \sqrt{2\beta^{-1} m_\alpha^\lambda(z(\tau))}\, \eta_\alpha(\tau), \tag{36}$$

where $\eta_\alpha(\tau)$ is a white-noise satisfying $\langle \eta_\alpha(\tau)\eta_\beta(\tau')\rangle = \delta_{\alpha\beta}\delta(\tau - \tau')$. To avoid confusion, we stress that the time τ in (36) is artificial and that we do not claim that the dynamics of the $\theta_\alpha(\sigma)$ in the original Ising model can be approximated by the solution of (36). Simply, we observe that the reactive trajectories in (36) have some of the same statistical properties as those of the original Ising model and, in particular, they share the same committor function (this, of course, assumes that the collective variables $\theta_\alpha(\sigma)$ are good collective variables and that (21) holds).

Why is this observation useful? It is useful because we know a lot about the mechanism of the reaction in the system governed by (36) (and thereby about the solution of (35)), at least when the temperature $1/\beta$ (i.e. the thermal energy) is much smaller than the free energy barriers between the metastable sets a and b. When this is the case, indeed, the theory of large deviations [15] (see also [4,16]) tells us that, with probability close to 1, the reactive trajectories follow the minimum free energy path (MFEP) between a and b, i.e. the curve, connecting the minimizer of $F_\lambda(z)$ in a to the one in b, which is such that it is always parallel to the vector field with components

$m_\alpha^\lambda(z)\partial F_\lambda(z)/\partial z_\alpha$. (More precisely, the theory tells us that the flux carried by the probability current of the reactive trajectories is concentrated in a small tube around the MFEP). If we parametrize the MFEP by $z(s)$ with $s \in [0, 1]$ and $|z'(s)| = cst$ (this corresponds to parametrizing the MFEP by normalized arc-length), $z(s)$ then satisfies

$$0 = m_\alpha^\lambda(z(s))\frac{\partial F_\lambda(z(s))}{\partial z_\alpha} - |z'(s)|^{-2} z'_\alpha(s) \sum_{\beta=1}^{M_B} z'_\beta(s) m_\beta^\lambda(z(s)) \frac{\partial F_\lambda(z(s))}{\partial z_\beta}, \qquad \alpha = 1, \ldots, M_B \quad (37)$$

where $z'(s) = (dz_1(s)/ds, \ldots, dz_{M_B}(s)/ds)$ is the string tangent at s.

In Sect. 3.4 we explain how to identify the MFEP solution of (37) via the string method. Before doing so, however, it is useful to give an expression for the committor function in terms of the MFEP. As explained in Ref. [4], locally around the MFEP, the committor function $\bar{Q}(z)$ solution of (35) takes constant value in the hyperplanes $P(s)$ whose normal $\hat{n}(s)$ is parallel to the gradient of the free energy, i.e. $\hat{n}(s) = \nabla_z F_\lambda(z(s))/|\nabla_z F_\lambda(z(s))|$. In addition, the committor function along the MFEP is given by [4]

$$\bar{Q}(z(s)) = \frac{\int_0^s R(s')/W(s')ds'}{\int_0^1 R(s')/W(s')ds'}. \quad (38)$$

Here

$$R(s) = \frac{|z'(s)|}{|m^\lambda(z(s))\hat{n}(s)|} \quad (39)$$

and

$$W(s) = \int_{P(s)} e^{-\beta F_\lambda(z)} d\sigma(z) \approx G(s) e^{-\beta F_\lambda(z(s))} \quad (40)$$

where $d\sigma(z)$ is the surface element in the hyperplane $P(s)$, and to obtain the last approximation in (40), we have used the fact that $e^{-\beta F_\lambda(z)}$is strongly peaked at $z(s)$ in $P(s)$, so that the integral can be evaluated by Laplace method. $G(s)$ is a prefactor term that accounts for the curvature of $F_\lambda(z)$ in $P(s)$ around $z(s)$. In this paper, we will neglect entropic effects associated with $G(s)$ and assume that $G(s) \approx cst$. Using (40) in (38) we then have

$$\bar{Q}(z(s)) = \frac{\int_0^s R(s') e^{\beta F_\lambda(z(s'))} ds'}{\int_0^1 R(s') e^{\beta F_\lambda(z(s'))} ds'}. \quad (41)$$

We will verify a posteriori that the assumptions that led to (41) (in particular $G(s) \approx cst$) are valid by checking how good an approximation $\bar{Q}(z(s))$ is of the committor function along the MFEP. Note that, if the free energy barrier along $z(s)$ is much higher

than $1/\beta$, the function $\bar{Q}(z(s))$ will vary sharply [4] from 0 to 1 at the point $z^\star$ along the MFEP where $F_\lambda(z(s))$ reaches its maximum, i.e. $F_\lambda(z^\star) = \max_{s\in[0,1]} F_\lambda(z(s))$. This point will then identify the transition state for the phase transformation.

3.4 String method

Let us denote by $g(z)$ the vector with components $g_\alpha(z) = -m_\alpha^\lambda(z)\partial F_\lambda(z)/\partial z_\alpha$. The basic idea of the string method is to identify the MFEP by evolving a curve using $g(z)$ as velocity for this curve while controlling its parametrization. In practice, this is done by starting from an initial guess for the string, $z(s,0)$, discretizing it into $P+1$ images $z_\alpha^p(0) = z_\alpha(p/P, 0)$, $p = 0,\ldots,P$, and, for $k = 0, 1, 2, \ldots$, updating these images as follows (for details, see e.g. [17]):

1. Evolve each image $z^p(k\Delta t)$ using the forward Euler scheme, i.e. compute

$$z_\alpha^{p,\star} = z_\alpha^p(k\Delta t) + g_\alpha(z^p(k\Delta t))\Delta t \tag{42}$$

   where Δt is the updating time-step.
2. Get a new set of images $z^p((k+1)\Delta t)$, $p = 0,\ldots,P$ by interpolating a piecewise linear curve across the points $z^{p,\star}$, $p = 0,\ldots,P$ and redistributing these points evenly along this curve (this enforces the discrete equivalent of parametrizing the curve by normalized arc-length).
3. Go to 1. unless some convergence criterion on $z^p((k+1)\Delta t)$ is satisfied.

The updating step in (42) requires one to know $g_\alpha(z) = -m_\alpha^\lambda(z)\partial F_\lambda(z)/\partial z_\alpha$. How to compute this term is explained next.

3.4.1 Calculation of the mean force and $m^\lambda(z)$

From (29), the factor $m_\alpha^\lambda(z)$ is a conditional average on the distribution (30). It is easy to show that the mean force $\partial F_\lambda(z)/\partial z_\alpha$ is also one such conditional average:

$$\frac{\partial F_\lambda(z)}{\partial z_\alpha} = \lambda\langle z_\alpha - \theta_\alpha(\sigma)\rangle_{\rho_{\lambda,z}}. \tag{43}$$

To compute these averages we use the Monte Carlo procedure described in Sect. 2.2 with $H(\sigma)$ replaced by the extended Hamiltonian $H_{\lambda,z}(\sigma)$ defined in Eq. (31). Explicitly, for each image independently, we compute

$$\frac{\partial F_\lambda(z^p(k\Delta t))}{\partial z_\alpha} \approx \frac{1}{N_k}\sum_{n=1}^{N_k} \lambda\left(z_\alpha^p(k\Delta t)) - \theta_\alpha(\sigma(n))\right). \tag{44}$$

Here N_k is the number of Monte Carlo steps performed at iteration k, with each step corresponding to an attempt to flip a randomly chosen spin, and $\sigma(n)$ is the spin state at step n. Similarly, the factor $m^\lambda(z)$ can be calculated using the estimator

$$m_\alpha^\lambda(z^p(k\Delta t)) \approx \frac{1}{N_k}\sum_{n=1}^{N_k} A_\alpha(n), \tag{45}$$

where we have introduced

$$A_\alpha(n) = \sum_{j\in J_\alpha} c(\sigma(n), \sigma^j(n)) \tag{46}$$

(with σ^j defined in (5)).

In practice the computation of the averages (44) and (45) is done in the following manner. At each iteration, we keep $z(k\Delta t)$ fixed, and evaluate (44) and (45) by an average of length $N_k = N_0(1+2\nu\Delta t)^k$ with $\nu > 0$. The reason why we progressively increase the length of the average is to guarantee that the string actually converges. If N_k was kept fixed, the string would keep oscillating due to statistical fluctuations in the estimator of $g(z)$. In contrast, by increasing the length of the averaging window as we do, the error on the estimators of the mean force and m^λ decreases as $N_0^{-1/2}(1+2\nu\Delta t)^{-k/2}$, which for $k = \lfloor t/\Delta t \rfloor$ is approximately $N_0^{-1/2}e^{-\nu t}$. Ideally, the constant ν should thus be chosen such that it matches the convergence rate of the exact iteration scheme, i.e. the one in which we would use the exact $g(z)$ rather than its approximation tainted by statistical error. If we take ν smaller than this convergence rate, the overall convergence will be limited by ν itself; if we take ν bigger than this convergence rate, then we waste computation time evaluating the averages too precisely at every step. In practice, ν was adjusted by trial and error in the results presented below.

Finally, we note that, from a computational point of view, the string method is rather easy to parallelize, since the evolution step (including the calculation of (44) and (45)) in (42) is carried out independently for each image, and only the reparametrization step requires information from all the images on the string.

3.4.2 Calculation of the free energy profile along the MFEP

Once the string has converged to the MFEP, the free energy along the MFEP can be calculated from the mean force using thermodynamic integration:

$$F_\lambda(z(s)) - F_\lambda(z(0)) = \int_0^s \sum_{\alpha=1}^{M_B} z'_\alpha(s')\frac{\partial F_\lambda(z(s'))}{\partial z_\alpha} ds'. \tag{47}$$

It is convenient to transform this expression into a new one more suitable for the computation because it only requires one to know the orientation of $z'(s)$ with respect to $g(s)$ and not its precise value (and hence it is less sensitive to small errors in the numerical approximation of $z'(s)$). To get this new expression, note that, along the MFEP, $z'(s)$ is parallel or antiparallel to $g(z(s))$, i.e.

$$z'_\alpha(s) = r(s)g_\alpha(z(s))\frac{|z'(s)|}{|g(z(s))|} \tag{48}$$

where $r(s) = +1$ if $\sum_{\alpha=1}^{M_B} g_\alpha(z(s))z'_\alpha(s) \leq 0$ and $r(s) = -1$ otherwise. Inserting (48) in (47) yields

$$F_\lambda(z(s)) - F_\lambda(z(0)) = \int_0^s \frac{r(s')}{|g(z(s'))|} \sum_{\alpha=1}^{M_B} g_\alpha(z(s')) \frac{\partial F_\lambda(z(s'))}{\partial z_\alpha} |z'(s')| ds'. \quad (49)$$

This formula can be discretized by trapezoidal rule

$$F_\lambda(z^p) - F_\lambda(z^0) = \frac{1}{2} \sum_{p'=1}^{p} (T^{p'} + T^{p'-1})|z^{p'} - z^{p'-1}| \quad (50)$$

where

$$T^p = \frac{r(p/P)}{|g(z^p)|} \sum_{\alpha=1}^{M_B} g_\alpha(z^p) \frac{\partial F_\lambda(z^p)}{\partial z_\alpha} \quad (51)$$

and $r(p/P) = -\text{sign}\left(\sum_{\alpha=1}^{M_B} g_\alpha(z^p)(z^{p+1} - z^{p-1})\right)$. Once the values $F_\lambda(z^p) \equiv F_\lambda(z(p/P))$ for $p = 0, \ldots, P$ have been obtained via (50), we compute $F_\lambda(z(s))$ on a finer grid in $s \in [0, 1]$ using cubic spline interpolation. This interpolation step turns out be useful because the free energy in the examples treated in Sect. 4 spans a rather large range of values and can vary significantly between the original points z^p. Interpolation between these points allows us to capture these variations at least to some degree of accuracy.

3.4.3 Calculation of the committor function along the MFEP

The values of the committor function along the MFEP, $\bar{Q}(z(s))$, can be calculated by discretizing (41) and using the interpolated $F_\lambda(z(s))$ computed in Sect. 3.4.2.

4 Results

In this section, we present the results of the string method applied to the study of the mechanism of the dynamics of phase transitions in the two-dimensional ferromagnetic Ising model consisting of a square lattice of $N_s = 100^2$ spins subject to different boundary conditions (Sects. 4.2 and 4.3). To begin, however, we test the continuous approximation made in Sect. 3.2 and determine the value(s) of λ required for this approximation to be valid.

4.1 Validation of the continuous approximation

In this section we check that, given the size of the block that we use to define the collective variables, there is indeed a range of values of the parameter λ such that the free

energy $F_\lambda(z)$ defined in (28) is roughly independent of λ. Recall that λ is the parameter that we use to smear things on the scale $(\beta\lambda)^{-1/2}$ using the factor $e^{-\beta\frac{\lambda}{2}|z-\theta(\sigma)|^2}$. If λ is too small, we expect that the smearing will be too aggressive, i.e. we will loose important features of the transition mechanism we wish to describe. But if λ is too big and the inequality (33) is not satisfied, the smearing will be ineffective and $F_\lambda(z)$ will not be the smooth function required in order that the continuous approximation made in Sect. 3 be valid.

The test we use is the following. We consider a system of spins of size $N_s = 100^2$ with periodic boundary conditions, in which the collective variables are defined using blocks of size $N_s^B = 100$, so that there are $M_B = N_s/N_s^B = 100$ collective variables. We also set the temperature at $1/\beta = 0.8/\beta_c$, i.e. below the transition temperature, and $h = 0$. (N_s, N_s^B, and $1/\beta$ are the same as what we will use in Sects. 4.2 and 4.3.) We then construct the following path in the space of the collective variables: $z_\alpha(s) = s$ for $\alpha = 1, \ldots, M_B$, where $s \in [0, 1]$. Note that this is not the MFEP, just an arbitrary path. To take into account admissible and not-admissible values for $\theta(\sigma)$, we discretize this path into $P = 2N_s^B$ points. At each point, we perform a Monte-Carlo run of 10^8 steps during which we calculate the estimator of $\nabla_z F_\lambda(z)$ according to (44) using different values of λ. We then compute the free energy as function of s by thermodynamic integration of $\nabla_z F_\lambda(z(s))$ along the path. This gives $\tilde{F}_\lambda(s) \equiv F_\lambda(z(s))$, which we normalize so that

$$\int_0^1 e^{-\beta\tilde{F}_\lambda(s)} ds = 1. \tag{52}$$

The function $\tilde{F}_\lambda(s)$ is shown in Fig. 4 for different values of λ. As it can be seen from this figure, there is range of values of λ around $\lambda = (N_s^B)^2/(4\beta) = 4{,}500$, roughly $4{,}000 \leq \lambda \leq 18{,}000$, for which $\tilde{F}_\lambda(s)$ is approximately independent of λ. In contrast, for $\lambda < 4{,}000$ and $\lambda > 18{,}000$, $\tilde{F}_\lambda(s)$ varies with λ. In particular, when $\lambda > 18{,}000$, the discreteness of the collective variables starts to emerge. This is reflected by $\tilde{F}_\lambda(s)$ displaying an oscillatory behavior, with local minima at the admissible points along the path, i.e. at $z_\alpha = n(2/N_s^B)$ with $n \in \mathbb{Z}$, and local maxima at the values of z_α that are not admissible for $\theta_\alpha(\sigma)$. The period of these oscillations in s is $2/N_s^B$ and their amplitude increases with increasing λ.

These results suggest that we should choose a value of λ in the range $4{,}000 \leq \lambda \leq 18{,}000$. However, since the variance of the estimator of the mean force (44) increases as λ [4], it is convenient to take λ not too big in this range. For the simulations presented in Sects. 4.2 and 4.3 we used $\lambda = (N_s^B)^2/4\beta = 4{,}500$.

4.2 Application I: Fixed boundary conditions

In our first application, we consider a two-dimensional system of $N_s = 100^2$ spins at $1/\beta = 0.8/\beta_c$, with no applied field ($h = 0$) and with fixed boundary conditions constructed in the following manner. Four additional layers of fixed spins are added around the system, where all spins in the upper and lower boundary layers are kept

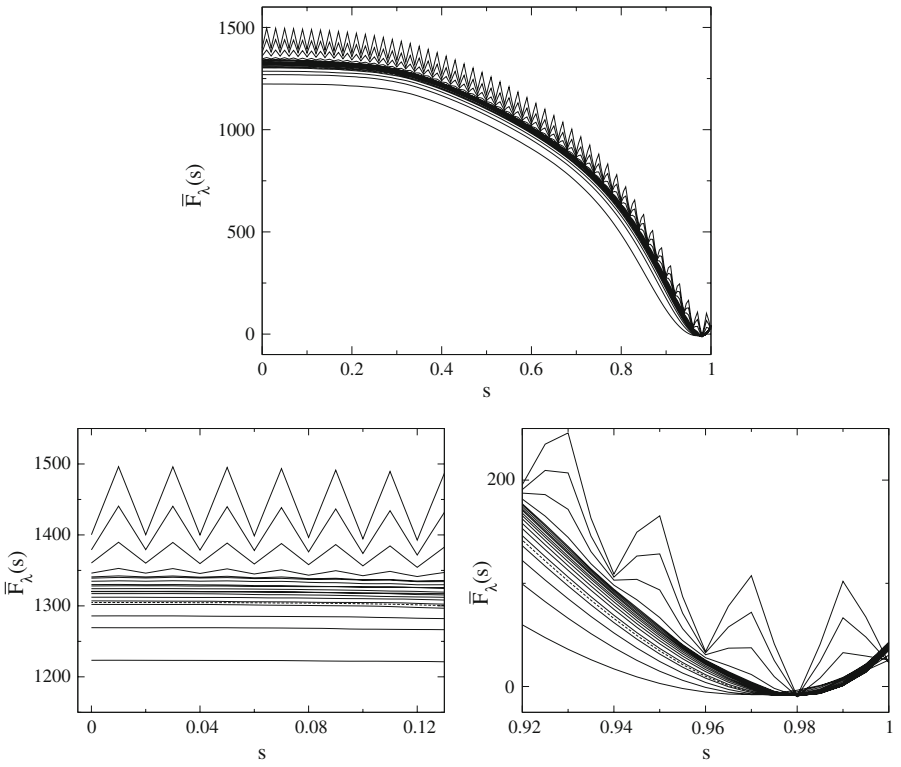

Fig. 4 The function $\tilde{F}_\lambda(s)$ as a function of s for various values of λ (top figure). The bottom figures show details of $\tilde{F}_\lambda(s)$ near $s = 0$ (left) and $s = 1$ (right). The values of λ go from 1,000 to 15,000 in steps of 1,000 and then from 20,000 to 50,000 in steps of 10,000, with curves at lower λ laying below the curves at higher λ. The dashed line is for the value $\lambda = (N_s^B)^2/(4\beta) = 4{,}500$. These results confirm the existence of a range of values for λ, roughly $4{,}000 \leq \lambda \leq 18{,}000$, for which $\tilde{F}_\lambda(s)$ is approximately independent of λ

fixed at the value $\sigma = -1$ and all spins in the left and right boundary layers at the value $\sigma = +1$, as illustrated in Fig. 5.

These fixed spins act as a local field on the system, in the sense that they contribute to the Hamiltonian in (1), but are kept fixed during the dynamics.

In this set-up, there are two equivalent (by symmetry) metastable states in the system (see Fig. 6) [18], one with positive magnetization close to $+1$ except for a thin layer near the upper and lower edges of the system (state A) and one with negative magnetization close to -1 except for a thin layer near the right and left edges of the system (state B). We are interested in studying the transition mechanism between these two metastable states.

4.2.1 String method set-up

To use the string method, we introduce $M_B = 100$ collective variables, each defined as in (20) with $N_s^B = 100$. As initial string we take a linear interpolation between the state

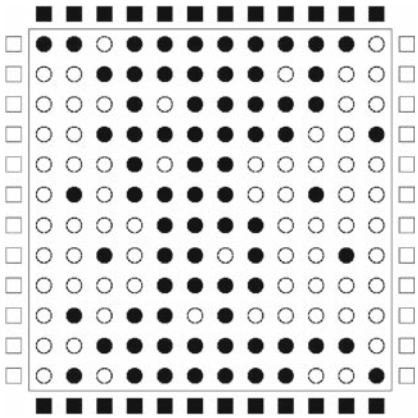

Fig. 5 Schematic representation of the fixed boundary conditions described in the text. Only the spins represented by circles (black: −1, white +1) are evolved according to the Metropolis dynamics, while the spins represented as squares are kept fixed at the value −1 (black squares) and +1 (white squares), and act as a local field on the neighboring spins. Note that it is not necessary to place spins at the four outer corners of the system since each spin interacts only with the four nearest neighboring spins

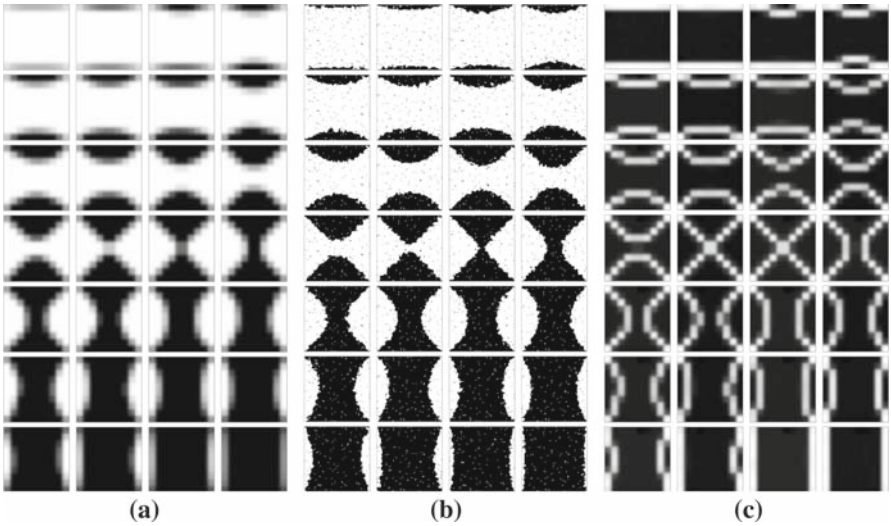

Fig. 6 (**a**) MFEP in the collective variables space for the Ising model with fixed boundary conditions. The MFEP goes from top left to bottom right, and is represented using 28 images. A grey-scale color coding is used, with white: +1 and black: −1. (**b**) Instantaneous spin configurations along the MFEP (white dots represent $\sigma = 1$ and black dots $\sigma = -1$). (**c**) Values of $m^{\lambda}(z)$ along the MFEP, color coded with black for the lowest values (≈ 3) and white for the highest values (≈ 16)

with $z_\alpha = 1$, and the state with $z_\alpha = -1$, $\alpha = 1, \ldots, M_B$, which we discretize into $P + 1 = 28$ images. The string is then evolved according to the procedure described in Sect. 3.4 with $\Delta t = 10^{-4}$ in (42). To calculate the estimators of the mean force and $m^{\lambda}(z)$ we used $\nu = 1.15$ and $N_0 = 10^7$. The initial string converged to the MFEP in about 8,000 iterations, and 2,000 more iterations were used to refine the MFEP.

4.2.2 Minimum free energy path

The MFEP in the space of the collective variables identified by the string method is shown in Fig. 6a, where the images along the path go from top left to bottom rigth. Figure 6b shows snapshots of corresponding instantaneous configurations of the spins, while the values of $m^{\lambda}(z)$ along the MFEP are represented in Fig. 6c. Note that $m^{\lambda}(z)$ is small (darker color) in the bulk and larger (lighter color) at the interfaces between blocks with opposite magnetization, so that it may be regarded as an interface tracker. Starting from the configuration with most spins up ($p = 0$), two clusters of spins down start to grow symmetrically from the boundaries fixed at the value -1. The clusters keep growing in size, until they merge at the center of the lattice, and form an X-shaped configuration ($p = 14$). At this point, the cluster of spins down starts to grow sidewise, towards the boundary layers with positive valued spins.

Although the system configurations in some of the points along the MFEP are not perfectly symmetric (see, e.g., $p = 21$ and 25), the MFEP is very reasonable and shows a symmetric transition pathway, as expected. The symmetry is two-fold: each configuration along the path is left-right and up-down symmetric due to the symmetric boundary conditions, and the path itself is symmetric by reversal of its direction and inversion of the sign of all the spins since the two end-points of the string have the same (free) energy, and are exactly equivalent by spin inversion.

Note finally that this transition pathway is strikingly similar to the one found in [16] in the context of Allen–Cahn equation (i.e. a partial differential equation which can be thought of as a mean field model for the Ising model).

4.2.3 Free Energy and committor test

The free energy profile along the MFEP, $F_{\lambda}(z(s))$, calculated using the procedure described in Sect. 3.4.2, is plotted in Fig. 7 (left). The free energy profile is approx-

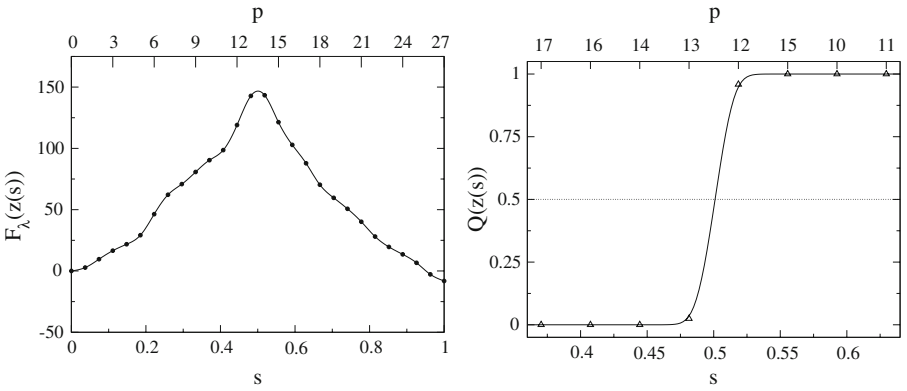

Fig. 7 Free energy profile and committor values along the MFEP for the spin system with fixed boundary conditions. The free energy (left figure) was calculated with (50) using the 28 points along the discretized MFEP (circles), and interpolated by cubic splines (full line). The committor (right figure) calculated using the cubic spline interpolation of the free energy (full line) agrees remarkably well with the committor values obtained by direct simulation (triangles)

imately symmetric, as expected from the symmetry of the MFEP, with two equally deep minima at the end points, separated by a high barrier located at $s = 0.5$ (i.e. between images $p = 13$ and $p = 14$—recall that we use cubic spline interpolation to get $F_\lambda(z(s))$ for $s \in [0, 1]$ from $F_\lambda(z^p)$ with $p = 0, \ldots, 27$).

In Fig. 7 (right) the committor values along the MFEP calculated using (41) are compared with the ones obtained by direct simulation, i.e. by creating a set of 500 different initial states of the spin system for every z^p along the MFEP (this is done by Monte Carlo sampling using the extended Hamiltonian $H_{\lambda,z^p}(\sigma)$), launching unrestrained trajectories from these initial states (i.e. using now the original Hamiltonian $H(\sigma)$), and calculating for every z^p the fraction of the 500 trajectories which reach first state B rather than A. The committor values from direct simulation are in very good agreement with the curve obtained using the cubic spline interpolation of the free energy, indicating that the collective variables are appropriate to describe the transition. Both give a committor value $\frac{1}{2}$ at $s = 0.5$ (i.e. between images $p = 13$ and $p = 14$), which is also the point for which the free energy has a maximum, and which corresponds to an X-shaped configuration of the system (see Fig. 6). This configuration can therefore be identified as the transition state.

4.3 Application II: Periodic boundary conditions

In the second application we consider a system similar to the one studied in Sect. 4.2 (same number $N_s = 100^2$ of spins at the same $1/\beta = 0.8/\beta_c$), but we change the boundary conditions to periodic boundary conditions and we turn on an uniform external field, $h \geq 0$. Our aim is to investigate in which way the presence of this external field changes the transition mechanism. In absence of an external field ($h = 0$) the two metastable states A and B have the same equilibrium distribution (2) and are equiprobable. When a positive uniform magnetic field is applied to the system, $h > 0$, the probability of state A decreases, while the one of B increases. There is a limiting value, function of the temperature, of the external field, above which the transition from state A to state B is no longer an activated process, i.e. the free energy barrier disappears. We are interested in what happens for values of h smaller than this critical value. The results presented in the following are for $h = 0.0$, 0.005, 0.01, 0.02, 0.03 and 0.04, since we established by Monte Carlo simulations that state A is no longer metastable around $h = 0.05$ when $1/\beta = 0.8/\beta_c$.

We apply the string method using the parameter setting described in Sect. 4.2.1.

4.3.1 Minimum free energy path

The results of our MFEPs calculations are shown in Fig. 8. The MFEPs at different values of h are represented in the space of the spins, with each MFEP going from top left to bottom right. The MFEPs in the collective variables space (not shown) are similar to the MFEPs in the space of the spins, only with a coarser resolution.

All the transition pathways involve the formation of a small circular-shaped droplet of the phase with all spins up into the bulk phase of spins down. This initial droplet

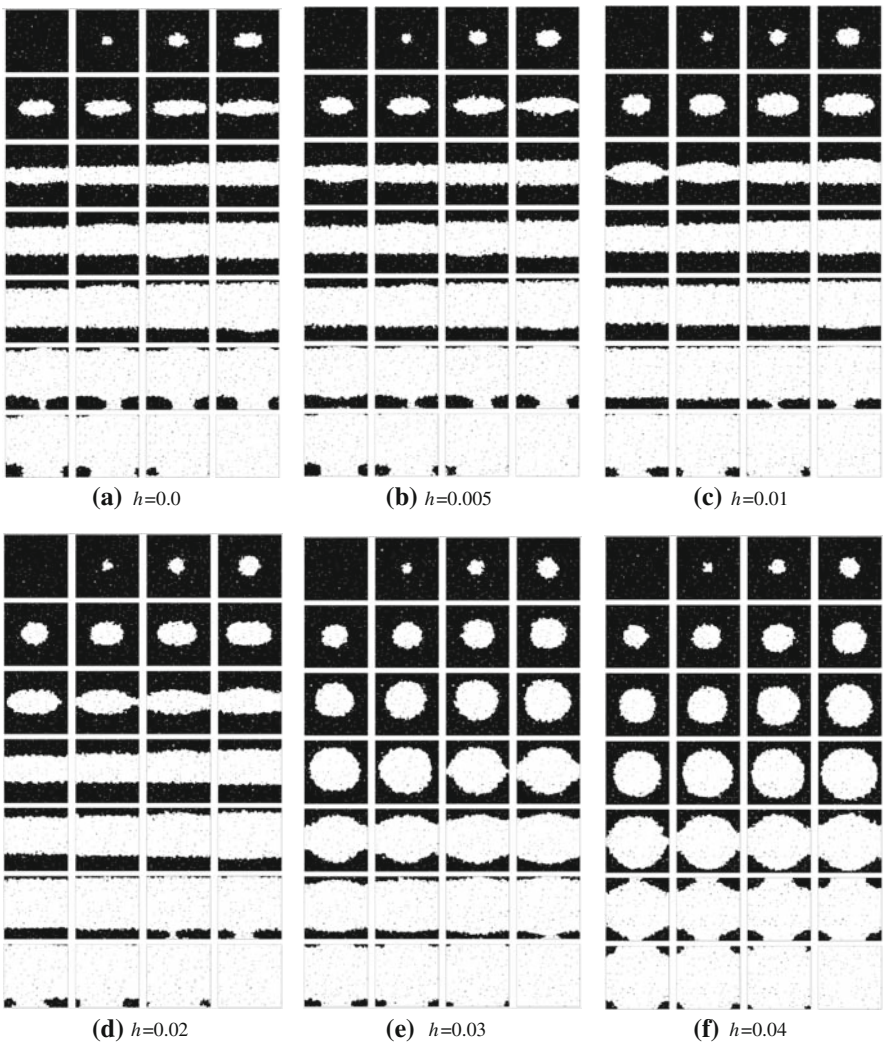

Fig. 8 MFEPs in the Ising system with periodic boundary conditions at increasing magnitude of the external magnetic field h. The MFEPs are represented in the space of the spins and each goes from top left to bottom right. Positive valued spins are represented in white and negative valued ones in black

then grows in a way which depends on the magnitude of the external applied field [19].

For $h \leq 0.02$, the droplet grows mainly horizontally first, until it reaches the left and right boundaries of the system and reconnects into a stripe-like structure. This stripe-like structure then grows by motion of its horizontal interfaces up to a point where it disconnects again into a droplet of spins down which then shrinks and evaporates. This transition from droplet to stripe is known as the percolative step in the phase transition

of the two and three dimensional nearest neighbor ferromagnetic Ising models (see e.g. [20]).

In contrast, for $h \geq 0.03$, the initial droplet remains approximately circular as it grows, until it reaches the left and right, then the upper and lower boundaries of the system. After the droplet has connected on all sides, the small remaining region of spins down evaporates.

To understand the difference in the transition mechanism at low and high values of the external field and to identify the transition state, we analyze the free energy profile along the MFEP and the committor values.

4.3.2 Free energy profiles, committor values and transition state

The free energy profiles and the committor values along the MFEPs are shown in Figs. 9 and 10, respectively. The committor values calculated using (41) are compared with the committor values obtained by direct simulation (triangles), where each point is a statistics on 500 unrestrained trajectories calculated as described in Sect. 4.2.3. To determine the "entropic contribution" to the transition pathway (this terminology is explained below) we have also calculated the committor values using (41) but replacing the free energy $F_\lambda(z(s))$ by the average Hamiltonian

$$E(z(s)) = \langle H(\sigma) \rangle_{\rho_{\lambda,z(s)}} \tag{53}$$

where $\langle \cdot \rangle_{\rho_{\lambda,z}}$ denotes conditional expectation with respect to (30), i.e. the approximate equilibrium expectation at $\theta(\sigma) = z$.

At all values of h the free energy along the MFEP displays two local minima corresponding to the metastable states A (i.e. $s = 0$, or image $p = 0$) and B (i.e. $s = 1$, or image $p = P$). At $h = 0$ the minima of the free energy have the same value, while as h is increased the free energy of B relative to A decreases, and the free energy barrier between A and B decreases.

For each value of h the free energy profile between the two minima can be divided into different regions, identified by a change of slope and indicated by vertical dotted lines in Fig. 9. For $h \leq 0.02$, there are two such changes of slope. Starting from $s = 0$ and moving toward $s = 1$, the first change of slope arises roughly when a configuration with a droplet (d) reconnects into one with a stripe-like structure going across the system (s), and the second change of slope arises when this elongated stripe breaks down into a droplet again. The first change of slope also coincides with the maximum of the free energy. In contrast, for $h \geq 0.03$, there are three changes of slope. Starting from $s = 0$ and moving toward $s = 1$, the first change, which also coincides with the free energy reaching its maximum, corresponds to no special change in configuration: it simply arises when the circular droplet reaches a critical size, which is bigger for $h = 0.03$ than for $h = 0.04$. The next two changes of slope then correspond to a droplet-to-stripe and a stripe-to-droplet transition, as observed for $h \leq 0.02$, with the difference that the free energy does not reach any maximum.

The transition at $h = 0$ is special since a flat energy profile is observed, roughly, for $s \in [0.26, 0.74]$ (i.e. between images $p = 7$ and $p = 20$). This indicates the presence of a diffusive free energy barrier, which corresponds to configurations where

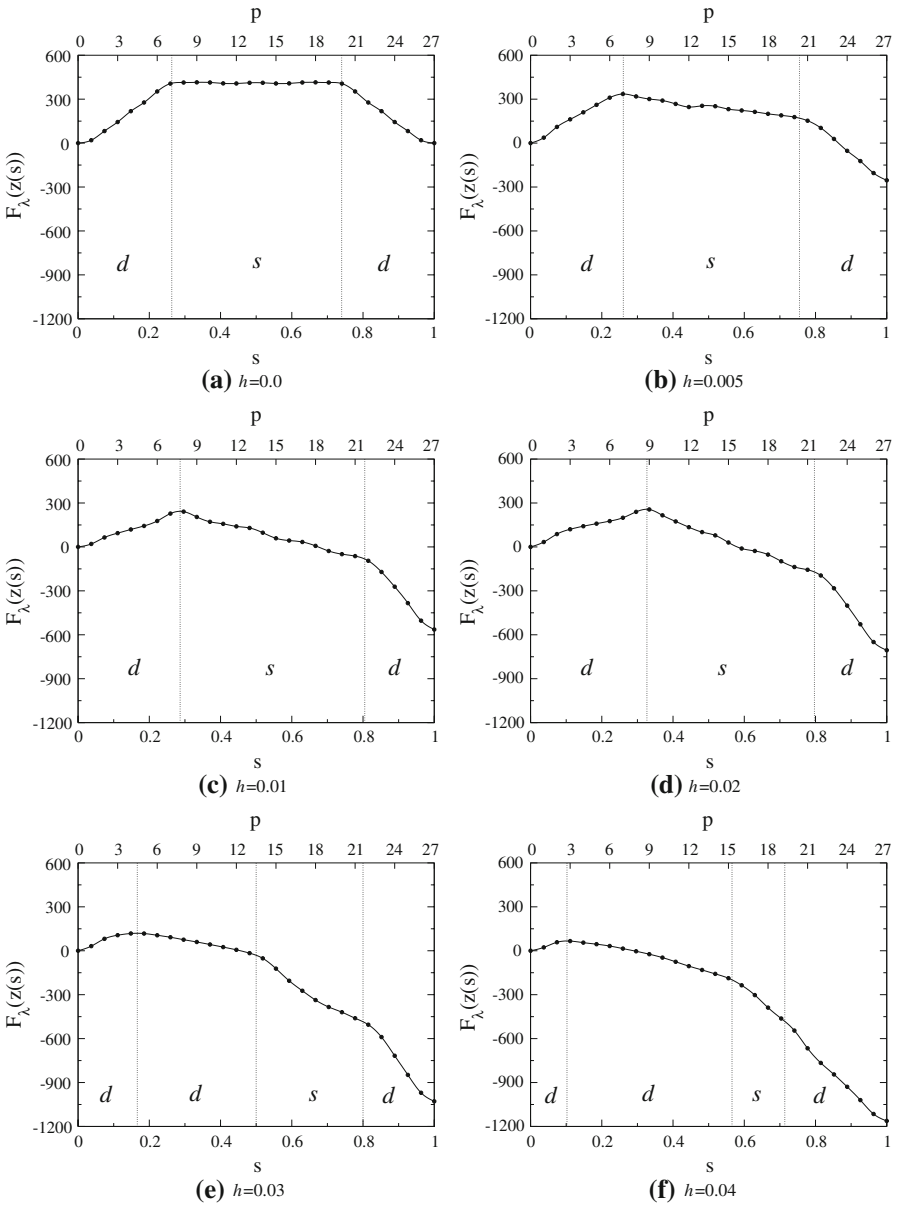

Fig. 9 Free energy profile along the MFEP for the system of spins with periodic boundary conditions at different values of the external magnetic field h. The free energy is calculated using the 28 images along the MFEP (black dots) and by cubic spline interpolation of these points (full line). The vertical dotted lines mark the boundaries of the regions where there is a droplet (d) in the system, or a stripe-like structure (s)

the spins separate into parallel stripes of opposite sign, as shown in Fig. 8a. Note that for this value of the field we symmetrized the free energy profile, since small errors in the MFEP calculation resulted in an unphysical asymmetry of the free energy profile. This diffusive region disappears at $h > 0$.

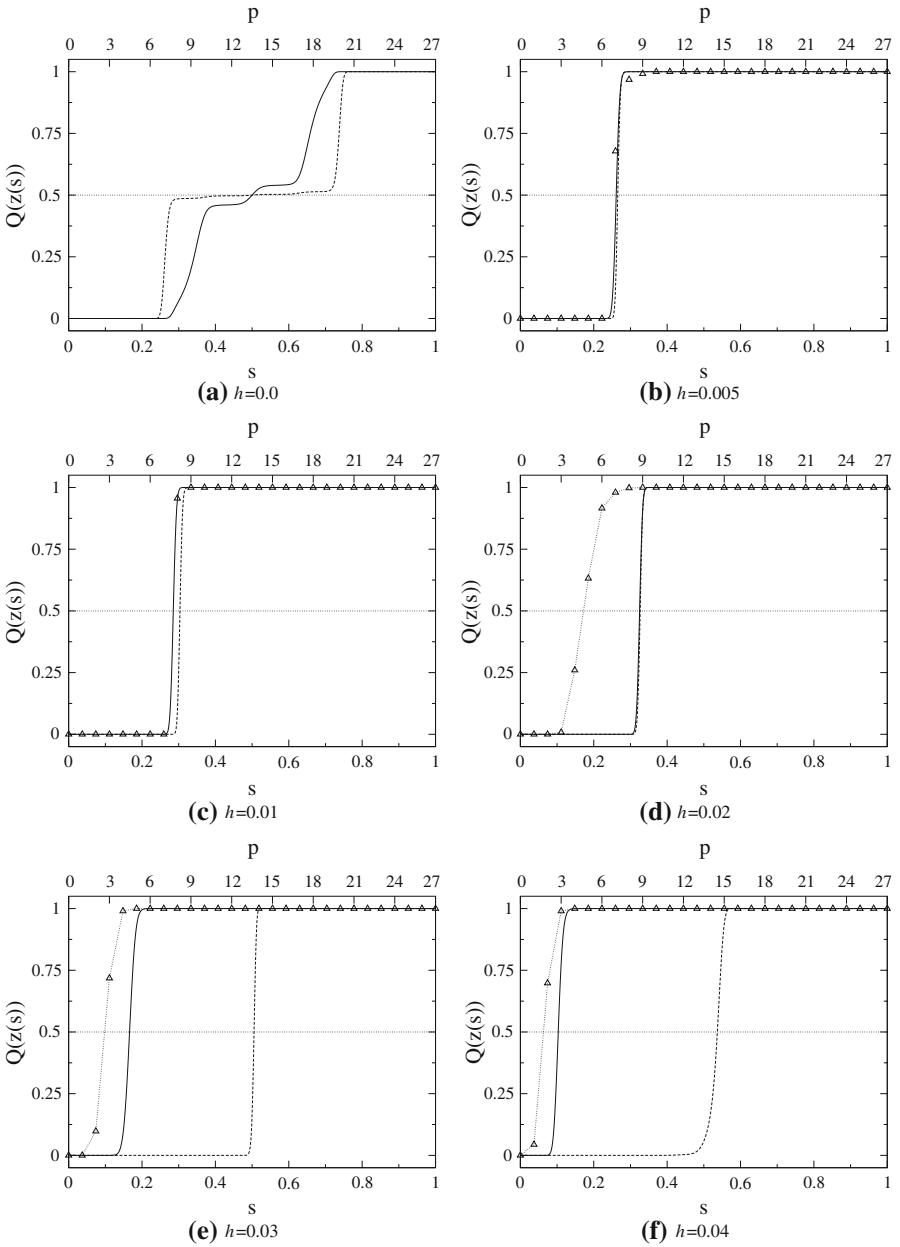

Fig. 10 Committor values along the MFEPs for different values of the applied field h. The committor values are calculated using the cubic spline interpolation of the free energy (solid line), the energy (dashed line) and by direct simulation (triangles)

For all considered values of h the free energy barrier is high compared to $1/\beta$, hence the free energy maximum determines the location of the committor value $\frac{1}{2}$ along the MFEP, as can be seen from Fig. 10. Due to the diffusive barrier, when $h = 0$, we

could not get a reliable estimate of the committor from direct simulation, since the trajectories started from the configuration in the middle of the flat barrier take a very long time to reach either A or B. For $h = 0.005$ and $h = 0.01$, the committor values calculated using the free energy and the ones from direct simulations are in good agreement. This agreement is not as good for $h \geq 0.02$, with $h = 0.02$ being the worst case. Note also that the committor values calculated using the average energy (53) instead of the free energy in (41) also agree reasonably well with those from direct simulations when $h = 0.005$, $h = 0.01$ and $h = 0.02$ but they do not when $h = 0.03$ and $h = 0.04$: these predictions also become markedly worse than the committor values calculated using the free energy for $h = 0.03$ and $h = 0.04$.

To explain these features, we shall make the two following working assumptions, which are consistent with our results (the first is about the mechanism of the transition, the second about an artifact in the string method which will be confirmed in Sect. 5 along with a way to correct for it):

1. In an infinite system with $h > 0$ and $1/\beta < 1/\beta_c$, the transition state is a quasi-circular critical droplet whose radius decreases when $1/\beta$ and/or h increase. Considering now a system of finite size, this implies that there exist a critical value of the field which depends on the temperature, say, $h_c(\beta)$, at which the critical droplet is as large as the system itself. For $h > h_c(\beta)$, the critical droplet is smaller than the system, and the transition path from the metastable state A to this critical droplet will essentially be the same as in the infinite system. However, for $h \leq h_c(\beta)$, the droplet growing out of state A reconnects before being able to reach its critical size, and the transition state becomes a stripe-like structure connected through two sides of the system (see Fig. 11 for an illustration). In addition, the size and shape of the transition state with stripe-like structure observed below $h_c(\beta)$ depend less on the temperature than the size of the critical droplet observed above $h_c(\beta)$.
2. Working with collective variables in the string method amounts to artificially cooling down the system. This means that the string calculation done at temperature $1/\beta$ describes in fact what happens at an effective temperature $1/\beta_{\text{eff}} < 1/\beta$.

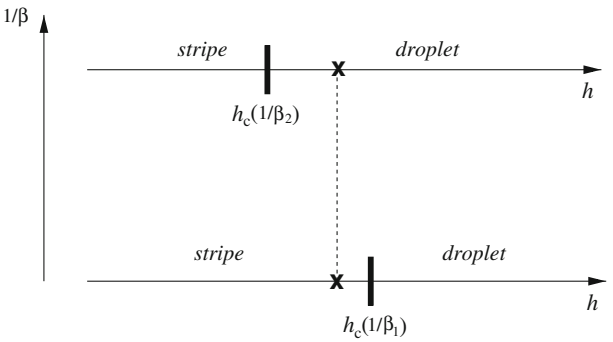

Fig. 11 Illustration of the switch in transition mechanism and the way the critical field at which this switch occurs depends on the temperature, here with $1/\beta_1 < 1/\beta_2 < 1/\beta_c$

Let us now show that we can put together these two working assumptions to explain our results. First, our results clearly corroborate the existence of a switch in the transition mechanism, with the transition state (i.e. the structure with committor $\frac{1}{2}$ along the MFEP) going from a stripe-like structure to critical droplet as h increases. However, they predict that the mechanism switch occurs at a larger value of the critical field than it actually does. This is because the string calculation corresponds to what effectively happens at some $1/\beta_{\text{eff}} < 1/\beta$ and the critical field at which the mechanism switch occurs depends on the temperature with $h_c(\beta_{\text{eff}}) > h_c(\beta)$ (see Fig. 11). According to what is seen in Fig. 10, it seems that $h_c(\beta)$ is somewhere between $h = 0.02$ and $h = 0.03$, whereas $h_c(\beta_{\text{eff}}) < 0.02$: this explains that the most important discrepancy between the committor predicted by the string method and the actual committor along the MFEP arises for $h = 0.02$. Below the mechanism switch, i.e. when $h = 0.005$ or $h = 0.01$ are less than both $h_c(\beta)$ and $h_c(\beta_{\text{eff}})$, the committor predicted by the string method agrees well with the actual committor, consistent with the transition state stripe-like structure being mostly independent of the temperature (and hence unaffected whether we work at the physical $1/\beta$ or the effective $1/\beta_{\text{eff}}$). Above the mechanism switch, the committor predicted by the string method is slightly off and to the right of the actual committor, i.e. the critical droplet predicted by the string method is slightly larger than the actual critical droplet along the MFEP. This is consistent with the size of the critical droplet depending on the temperature and being smaller at $1/\beta$ than $1/\beta_{\text{eff}}$. Note that, when the committor function calculated along the MFEP via the string method does not agree with the one estimated by direct simulation, the MFEP itself may be incorrect. In particular, the path in Fig. 8 when $h = 0.02$ is incorrect because the string method misses the mechanism switch due to the artificial cooling effect it introduces (the problem is less dramatic for the paths when $h = 0.03$ and $h = 0.04$ since the cooling effect does not interfere with the finite size of the system at these field values). The correct path when $h = 0.02$ is shown in Fig. 14 below and we explain in Sect. 5 how it can be obtained by compensating for the cooling effect of the string method.

The committor values predicted using the average energy, $E(z(s))$ in (53), rather than the free energy provide an additional confirmation of our working assumptions. Indeed, using $E(z)$ rather than $F_\lambda(z)$ amounts to cooling the system even more, and therefore amplifying the effects described above even further (Fig. 10 suggests that the effective temperature obtained by working with $E(z)$ is such that the critical field $h_c(\beta)$ at this temperature is even above $h = 0.04$).

Finally, it should be stressed that the MFEP is degenerate since the system is invariant by translation. Our results indicate that this degeneracy is not too important since it does not seem to affect much the committor function (at least after correcting for the cooling effect following the procedure discussed in the next section). This point, however, deserves further investigation.

5 Outlook and discussion

Our results show that the string method is able to compute efficiently and with good accuracy the MFEP and thereby capture the transition mechanism in the kinetics of

phase transformations in the Ising model under different conditions. This task would have been difficult and extremely costly to address by direct simulation, and even by other existing methods (such as umbrella sampling), due to the large number (= 100) of collective variables that we use to describe the transition. We have shown that these collective variables are indeed a good set of variables, not only because the MFEPs in these variables are very reasonable transition paths, but also (and more decisively) because they predict the committor function along this MFEP (and the associated transition state) with reasonable accuracy. These features make the technique attractive and potentially useful for more interesting and challenging applications than the Ising model. Nevertheless, we have noticed that, in some special cases, the string method gives an incorrect transition pathway. As already mentioned in Sect. 4.3 this effect is due to the fact that, as we discuss next, introducing collective variables amounts to artificially cool down the system. This also means that, in the string method, the results can be improved by working with an artificial temperature higher than the physical one. Let us elaborate on these points.

Let us first establish that using collective variables does indeed artificially cool the system down. To this end, consider a system of spins with periodic boundary conditions and $h = 0$, in which we introduce a constant number, $M_B = 100$, of collective variables but we change the number of spins N_s, so that the size of the blocks used to define the collective variables increases with increasing N_s, i.e. $N_s^B = N_s/100$. In each system, we identify the minimizer of the free energy $F_\lambda(z)$. This can be done, for instance, by starting from the initial condition $z_\alpha(0) = 1$, $\alpha = 1, \ldots, M_B$ and evolving the collective variables by steepest descent

$$z_\alpha((k+1)\Delta t) = z_\alpha(k\Delta t) - \frac{\partial F_\lambda(z(k\Delta t))}{\partial z_\alpha}\Delta t \tag{54}$$

where $\partial F_\lambda(z(k\Delta t))/\partial z_\alpha = \lambda\langle z_\alpha(k\Delta t) - \theta_\alpha(\sigma)\rangle_{\rho_{\lambda,z}}$, $\Delta t = 10^{-4}$, $1/\beta = 0.8/\beta_c$, and $\lambda = (N_s^B)^2/(4\beta)$. The fixed point of (54) is a configuration $z^\star$ minimizing the free energy. The average magnetization per spin, m, conditional on $\theta(\sigma) = z^\star$ (which we compute approximately using restraints) is plotted in Fig. 12 as a function of the size of the blocks, N_s^B. Our results show that m is higher than its value in a unrestrained system at the same temperature (dashed line in the figure), with m approaching the value of the unrestrained system with increasing size of the blocks. Since there is a one-to-one correspondence between average magnetization and temperature, this confirms that the restraint imposed by the collective variables results in an effective temperature which is lower than the physical temperature $1/\beta$ (i.e. the one used in the Monte Carlo dynamics) of the system.

This cooling effect is also shown in Fig. 13. Here we fix the size of the blocks at $N_s^B = 100$, and we compare the magnetization per spin as a function of temperature in a free system and in a system with the restraint on the collective variables. The figure also indicates which artificial temperature $1/\bar{\beta}$ should be used in the restrained simulations in order that the effective temperature $1/\beta_{\text{eff}} < 1/\bar{\beta}$ (which we determine via the average magnetization, m, it induces) be equal to the physical one, $1/\beta_{\text{eff}} = 1/\beta$.

These results suggest that the discrepancies that we observed in Sect. 4.3 between the actual committor function and the one calculated by the string method can be

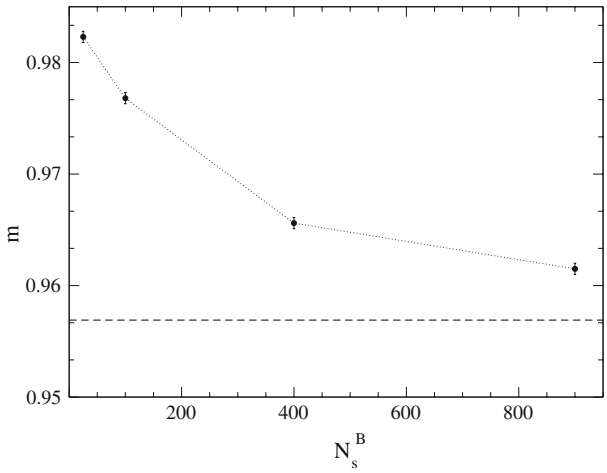

Fig. 12 Average magnetization per spin as a function of the number of spins in the blocks used to define the collective variables. The dashed line indicates the value of the magnetization in a unrestrained system at the temperature used in the restrained simulations ($1/\beta = 0.8/\beta_c$)

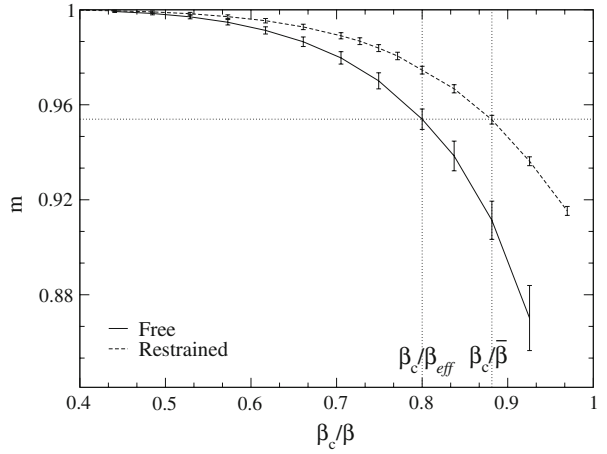

Fig. 13 Average magnetization per spin as a function of temperature for a free system (solid line) and a system with the restraint on the collective variables (dashed line). The dotted lines indicate how to determine the artificial temperature $1/\bar{\beta}$ to use in the restrained simulation in order that the effective temperature $1/\beta_{\text{eff}} < 1/\bar{\beta}$ in this system be equal to the physical temperature, $1/\beta_{\text{eff}} = 1/\beta$

diminished by using the string method at an artificially higher temperature so that $1/\beta_{\text{eff}} = 1/\beta$—from Fig. 13, it turns out that $1/\bar{\beta} = 0.87/\beta_c$ gives $1/\beta_{\text{eff}} = 1/\beta = 0.8/\beta_c$ and we checked that this result does not depend much on the applied field. We applied this technique to revisit the transition pathway at $h = 0.02$: the new pathway obtained by the string method using $1/\bar{\beta} = 0.87/\beta_c$ is shown in Fig. 14. Comparing this path to those shown in Fig. 8, we see that the new MFEP looks more like the ones in which the transition state is a critical droplet than those in which it is a

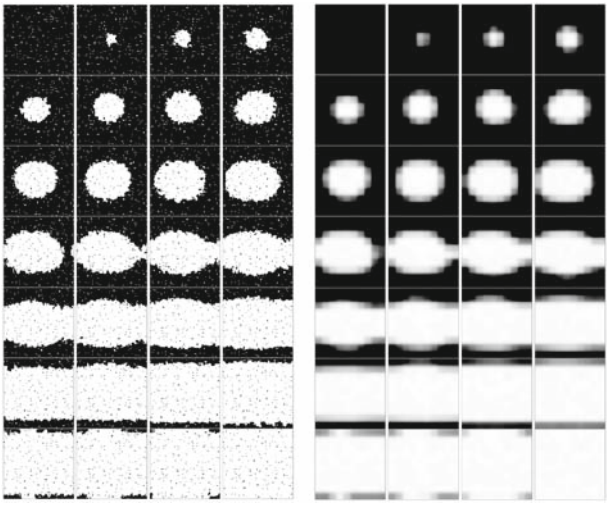

Fig. 14 MFEP (left: spin space, right: collective variable space) for the system with periodic boundary conditions and $h = 0.02$. The MFEP was calculated at the temperature $1/\bar{\beta} = 0.87/\beta_c$, which gives as effective temperature the desired temperature of $1/\beta_{\text{eff}} = 0.8/\beta_c$

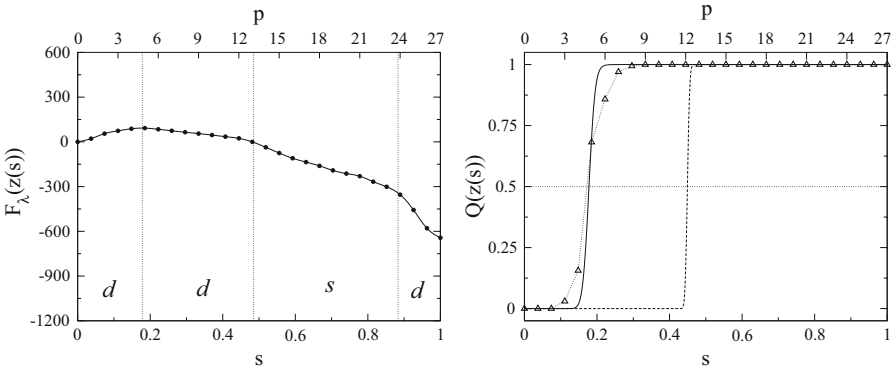

Fig. 15 Free energy profile and committor values along the MFEP for the spin system with periodic boundary conditions, $h = 0.02$ and $1/\bar{\beta} = 0.87/\beta_c$ (corresponding to $1/\beta_{\text{eff}} = 0.8/\beta_c$). The committor values from direct simulation (triangles) were computed using the images along the MFEP calculated at $1/\bar{\beta}$, but the initial spin configurations at each image for each of the 500 unrestrained simulations were sampled at $1/\beta_{\text{eff}}$. Each free simulation was then run at $1/\beta_{\text{eff}}$

stripe-like structure (i.e. we now correctly predict that we should be past the mechanism switch at $h = 0.02$). This is confirmed by the free energy profile shown in Fig. 15. The committor function shown in this figure now agrees much better with the one estimated by direct simulation. This shows that artificially increasing the temperature in a consistent way within the string method permits, to some extent, to correct for the artifact that the string method introduces if employed at the physical temperature. However, we should stress that the range of validity of this procedure is not completely

clear. A more satisfactory way to deal with this problem would be to use the finite temperature string method [12,21].

A Efficient calculation of some relevant quantities

In this Appendix we derive the explicit expressions for the update of $H(\sigma)$, $\theta(\sigma)$, $H_{\lambda,z}(\sigma)$ and $m^{\lambda}(z)$ when the state of the spin system is changed from σ to σ^j. We show that the changes in these quantities only depend on the state of the system at the previous MC step, and that their calculation only involves the spin which has changed sign and its nearest neighbors, so that they can be efficiently computed in a simulation.

A.1 Hamiltonian of the system of spins

We first rewrite the Hamiltonian in (1) as

$$H(\sigma(n)) = -J \sum_{\langle i,k\rangle \neq j} \sigma_i(n)\sigma_k(n) - h\sum_{i\neq j}\sigma_i(n) - \sigma_j(n)(J \sum_{i\in neigh_j} \sigma_i(n) + h) \quad \text{(A1)}$$

where the contribution of $\sigma_j(n)$ (with n denoting the current MC step) is made explicit and we have indicated by $neigh_j$ the indexes of the nearest neighboring spins of σ_j. If at step $n+1$ σ_j is flipped, the only term that changes in (A1) is the last term at the r.h.s., which becomes $+\sigma_j(n)(J\sum_{i\in neigh_j}\sigma_i(n)+h)$. Hence we have

$$H(\sigma(n+1)) = H(\sigma(n)) + 2\sigma_j(n)(J \sum_{i\in neigh_j} \sigma_i(n) + h). \quad \text{(A2)}$$

Note that all the quantities at the r.h.s. of the equality (A2) are evaluated at step n.

A.2 Collective variables

We now consider the collective variables defined via (20). Suppose that the variable $\theta_\alpha(\sigma)$ is defined in the block B_α which contains σ_j. We can then rewrite (20) as

$$\theta_\alpha(\sigma(n)) = \frac{1}{N_s^B}\sum_{\substack{i\in J_\alpha \\ i\neq j}} \sigma_i(n) + \frac{\sigma_j(n)}{N_s^B}. \quad \text{(A3)}$$

The first term at the r.h.s. of (A3) does not depend on spin j, hence when σ_j is flipped the new value of the collective variable in block B_α is simply given by

$$\theta_\alpha(\sigma(n+1)) = \theta_\alpha(\sigma(n)) - \frac{2\sigma_j(n)}{N_s^B} \quad \text{(A4)}$$

A.3 Restraining potential

To calculate the change in the restraining potential on the collective variables when $\sigma_j \in B_\alpha$ is flipped, we define $\tilde{H}_{\lambda,z}(\sigma) = H_{\lambda,z}(\sigma) - H(\sigma)$ and, using (31), write it as

$$\begin{aligned}\tilde{H}_{\lambda,z}(\sigma(n)) &= H_{\lambda,z}(\sigma(n)) - H(\sigma(n)) \\ &= \frac{\lambda}{2}\left(\sum_{\beta\neq\alpha}^{M_B}(\theta_\beta(\sigma(n)) - z_\beta)^2 + (\theta_\alpha(\sigma(n)) - z_\alpha)^2\right). \end{aligned} \tag{A5}$$

When spin σ_j is flipped, the only term that changes in (A5) is the term depending on the index α, so that we have

$$\begin{aligned}&\tilde{H}_{\lambda,z}(\sigma(n+1)) - \tilde{H}_{\lambda,z}(\sigma(n)) \\ &= \frac{\lambda}{2}\left(\theta_\alpha^2(\sigma(n+1)) - \theta_\alpha^2(\sigma(n)) - 2z_\alpha\left(\theta_\alpha(\sigma(n+1)) - \theta_\alpha(\sigma(n))\right)\right). \end{aligned} \tag{A6}$$

Using (A4) we obtain

$$\theta_\alpha^2(\sigma(n+1)) - \theta_\alpha^2(\sigma(n)) = -\frac{4\sigma_j(n)}{N_s^B}\left(\theta_\alpha(\sigma(n)) - \frac{\sigma_j(n)}{N_s^B}\right). \tag{A7}$$

Substituting (A4) and (A7) in (A6) gives as final result

$$\tilde{H}_{\lambda,z}(\sigma(n+1)) = \tilde{H}_{\lambda,z}(\sigma(n)) + \frac{2\lambda\sigma_j(n)}{N_s^B}\left(z_\alpha - \theta_\alpha(\sigma(n)) + \frac{\sigma_j(n)}{N_s^B}\right). \tag{A8}$$

A.4 Calculation of $m^\lambda(z)$

Recall that to estimate $m_k^\lambda(z)$ we have introduced the quantity (see (46))

$$A_\alpha(n) = \sum_{i\in J_\alpha} c(\sigma(n), \sigma^i(n)). \tag{A9}$$

The only terms that will change in the sum (A9) when σ_j is flipped are the ones depending on σ_j and the ones depending on spins σ_i with $i \in J_\alpha$ and $i \in neigh_j$. Explicitly

$$\begin{aligned}A_\alpha(n+1) - A_\alpha(n) \;&= -c(\sigma(n), \sigma^j(n)) + c(\sigma(n+1), \sigma^j(n+1)) \\ &\quad - \sum_{\substack{i\in neigh_j \\ i\in J_\alpha}} c(\sigma(n), \sigma^i(n)) + \sum_{\substack{i\in neigh_j \\ i\in J_\alpha}} c(\sigma(n+1), \sigma^i(n+1)). \end{aligned} \tag{A10}$$

Now note that by the definition in (5) the state of the spin system obtained from state $\sigma(n)$ by flipping spin σ_j satisfies $\sigma(n+1) = \sigma^j(n)$ (or, equivalently, $\sigma^j(n+1) = \sigma(n)$). So that we can rewrite the first term on the r.h.s. of (A10) as

$$\begin{aligned} -c(\sigma(n), \sigma^j(n)) + c(\sigma^j(n), \sigma(n)) &= -\min\left\{e^{-\beta(H_{\lambda,z}(\sigma^j(n))-H_{\lambda,z}(\sigma(n)))}, 1\right\} \\ &\quad + \min\left\{e^{\beta(H_{\lambda,z}(\sigma^j(n))-H_{\lambda,z}(\sigma(n)))}, 1\right\} \\ &= \begin{cases} -e^{-\beta\Delta H_{\lambda,z}} + 1 & \text{if } \Delta H_{\lambda,z} > 0 \\ -1 + e^{\beta\Delta H_{\lambda,z}} & \text{if } \Delta H_{\lambda,z} < 0 \\ 0 & \text{if } \Delta H_{\lambda,z} = 0, \end{cases} \end{aligned} \tag{A11}$$

where we have used the compact notation $\Delta H_{\lambda,z} = H_{\lambda,z}(\sigma^j(n)) - H_{\lambda,z}(\sigma(n))$. The factor $\Delta H_{\lambda,z}$ can be calculated using (A2) and (A8). The terms in the last line of (A10) can be updated in a similar manner, and only involve the neighboring spins of σ_j which belong to block B_α. Note, however, that the neighboring spins of σ_j could belong to blocks different than B_α. In that case it is the sum in the corresponding block that has to be updated.

Acknowledgements One of the authors (M.V.) was supported by the EC through the Marie Curie EST project MEST-CT-2005-020491, by CECAM (Lyon) and by US DARPA grant 25-74200-F6053. Part of this work was performed while one of the authors (M.V.) was a researcher at CECAM. We acknowledge CECAM for providing the computational resources used for this work.

References

1. P.R. ten Wolde, M.J. Ruiz-Montero, D. Frenkel, Phys. Rev. Lett. **75**, 2714–2717 (1995)
2. P.R. ten Wolde, M.J. Ruiz-Montero, D. Frenkel, J. Chem. Phys. **104**, 9932–9947 (1996)
3. C. Valeriani, E. Sanz, D. Frenkel, J. Chem. Phys. **122**, 194501 (2005)
4. L. Maragliano, A. Fischer, E. Vanden-Eijnden, G. Ciccotti, J. Chem. Phys. **125**, 024106 (2006)
5. T.F. Miller, E. Vanden-Eijnden, D. Chandler, Proc. Natl. Acad. Sci. USA **104**, 14559–14564 (2007)
6. E. Weinan, E. Vanden-Eijnden, J. Stat. Phys. **123**, 503–523 (2006)
7. E. Vanden-Eijnden, in *Transition path theory*. ed. by M. Ferrario, G. Ciccotti, K. Binder. Computer Simulations in Condensed Matter: From Materials to Chemical Biology, vol 1 (Springer, Berlin, 2006), pp. 439–478
8. K. Binder, Rep. Prog. Phys. **50**, 783–859 (1987)
9. P.A. Rikvold, B.M. Gorman, in *Recent results on the decay of metastable phases*. ed. by D. Stauffer. Annual Reviews of Computational Physics I (World Scientific, Singapore, 1994), pp. 149–192
10. L. Onsager, Phys. Rev. **65**, 117–149 (1994)
11. C.N. Yang, Phys. Rev. **85**, 808–816 (1952)
12. E. Weinan, W. Ren, E. Vanden-Eijnden, Chem. Phys. Lett. **413**, 242–247 (2005)
13. P. Metzner, C. Schütte, E. Vanden-Eijnden, Mult. Model. Simul, SIAM (2007)
14. G. Giacomin, J. L. Lebowitz, E. Presutti, in *Deterministic and stochastic hydrodynamic equations arising from simple microscopic model systems*. ed. by R.A. Carmona, B. Rozovskii. Stochastic Partial Differential Equations: Six Perspectives, volume Math. Surveys Monogr, vol 64 (AMS, Providence, RI, 1999), pp. 107–152
15. M.I. Freidlin, A.D. Wentzell, *Random Perturbations of Dynamical Systems* (Springer, Berlin-Heidelberg-New York, 1984)
16. E. Weinan, W. Ren, E. Vanden-Eijnden, Comm. Pure. Appl. Math. **57**, 637–656 (2004)
17. E. Weinan, W. Ren, E. Vanden-Eijnden, J. Chem. Phys. **126**, 164103 (2007)
18. A. Milchev, A. De Virgiliis, K. Binder, J. Phys.: Condens. Matter **17**, 6783–6804 (2005)

19. H.L. Richards, S.W. Sides, M.A. Novotny, P.A. Rikvold, J. Magn. Magn. Mater. **150**, 37–50 (1995)
20. A.L. Efros, *Physics and Geometry of Disorder* (MIR, Moscow, 1986)
21. E. Weinan, W. Ren, E. Vanden-Eijnden, J. Phys. Chem. B **109**, 6688–6693 (2005)